Research on Engineering Structures & Materials
www.jresm.org
MIM Research Group

Research Article

Enhancing tribological and machining performance in A356 hybrid composites through TOPSIS optimization

Vinothkumar S [1,a], Rajesh S [2,b], Preetham Reddy C. S [3,c], Arul N [4,d], Suyash Pawar [5,e], Mayakannan S [*,6,7,f]

[1]*Dept. of Mechanical Eng., Vel Tech Multi Tech Dr.Rangarajan Dr.Sakunthala Engineering College-Avadi, Chennai, India*
[2] *Dept. of Mechanical Engineering, Meenakshi college of engineering, Chennai, Tamilnadu, India*
[3]*Dept. of Electronics and Communication Eng., Koneru Lakshmaiah Education Foundation, Guntur, Andhra Pradesh, India*
[4]*Dept.of Mechatronics Eng., Sona College of Technology, Salem, Tamilnadu, India*
[5]*Dept. of Mechanical Eng., MVPS KBT Engineering College, Nashik, Maharashtra, India*
[6]*Dept.t of Mechanical Engineering, Saveetha School of Engineering, Saveetha Institute of Medical and Technical Sciences, SIMATS, Chennai, Tamil Nadu, India 602105*
[7]*Dept. of Mechanical Eng., Rathinam Technical Campus, Coimbatore, Tamilnadu, India*

Article Info

Article History:

Received 17 Feb 2025

Accepted 20 May 2025

Keywords:

Surface morphology;
TOPSIS;
Tribology;
Electrical discharge machining;
Optimization

Abstract

The tribological and machining characteristics of A356 hybrid composites supplemented with silicon nitride (Si_3N_4) and molybdenum disulfide (MoS_2) were examined to improve wear resistance and machinability. Stir casting was employed to create the composites, with MoS_2 varying from 0 to 10 wt%, while Si_3N_4 remained constant at 5 wt%. A Taguchi-based TOPSIS optimization method was utilized to assess the impact of reinforcement content, load, sliding speed, distance, and temperature on wear rate, coefficient of friction (CoF), and hardness. The performance of electric discharge machining (EDM) was evaluated utilizing used motor oil (UMO) as a dielectric to measure material removal rate (MRR), tool wear rate (TWR), and surface roughness (Ra). The findings indicated that 2 wt% MoS_2 yielded the minimal wear rate (0.00061 mg/min) and coefficient of friction (0.399) attributable to the development of a mechanically mixed layer (MML), but 6 wt% MoS_2 attained the maximum hardness (127 HRB). At elevated loads and temperatures (225°C, 70N), MML degradation resulted in delamination wear, exacerbating material loss. In EDM, the optimal surface roughness (Ra = 2.383 µm) was attained at 5 g/L alumina, 24 A current, and 50 µs pulse on-time, surpassing traditional A356 EDM machining. The application of UMO as a sustained dielectric enhanced MRR and TWR, indicating its feasibility for precision manufacturing. This research establishes that A356/Si_3N_4/MoS_2 hybrid composites provide superior wear resistance, optimum hardness, and enhanced machinability, rendering them appropriate for automotive, aerospace, and industrial applications.

1. Introduction

Aluminum composites excel in high-performance applications requiring strength, wear resistance, and thermal stability, but challenges like brittleness, machining difficulties, and cost must be addressed through advanced processing and material optimization [1]. A356 aluminum alloy is a lightweight, high-strength material extensively used in tribology and electrical discharge

*Corresponding author: kannanarchieves@gmail.com
[a]orcid.org/0000-0002-6060-6800; [b]orcid.org/0000-0001-5296-3333; [c]orcid.org/0009-0004-1039-3247; [d]orcid.org/0000-0002-8397-5633, [e]orcid.org/0000-0003-4776-4780, [f]orcid.org/0000-0002-3463-1965
DOI: http://dx.doi.org/10.17515/resm2025-690ma0217rs

machining (EDM) applications due to its superior mechanical properties and adaptability [2]. It exhibits excellent wear resistance and thermal conductivity, making it an ideal choice for components subjected to high friction and thermal load. Si_3N_4 was selected to enhance hardness, wear resistance, and mechanical strength, MoS_2 was added as a solid lubricant, reducing friction and wear by forming a low-shear tribofilm. The combination of Si_3N_4 (strength) and MoS_2 (lubrication) ensures improved tribological and mechanical properties, making the composite highly effective for high-performance applications [3]. A356 alloy, strengthened with fly ash and SiC was produced by stir-squeeze casting, resulting in a pore-free microstructure and enhanced mechanical characteristics. The composite with 10 wt% fly ash showed lower wear rates and friction under dry sliding, suitable for automotive and structural applications [4]. A356/CaB6 composites were produced with varying CaB6 contents, with the 5% reinforcement showing increased hardness, tensile strength, and reduced wear rate. The higher friction coefficient and low wear rate make it suitable for automotive applications [5]. A metal matrix composite (MMC) of A356 aluminum alloy with 4% tungsten carbide (WC) was fabricated using stir casting and examined for machining characteristics in wire EDM. Taguchi-fuzzy inference system (FIS) simulation and ANOVA were used to optimize dry turning parameters for cast A356 aluminum alloy, with depth of cut identified as the most significant factor on MRR and SR, achieving the optimal condition at high speed and depth of cut [6]. EDM process parameters were optimized for thixoformed A356-5TiB2 composites using fuzzy logic and GRA. This study assessed MRR and surface morphology, with SEM analysis revealing improved surface integrity under optimal conditions [7]. This study optimized ultrasonic-assisted stir casting parameters for Al6061 composites reinforced with nano Al_2O_3 and nano ZrO_2 using Taguchi L16 design. Analysis with S/N ratio, regression model, and Minitab 21 showed that stirring speed, temperature, time, and reinforcement content significantly influenced UTS [8]. Aluminum matrix composites with melon shell ash (0–20 wt.%) were fabricated from recycled cans. Maximum tensile strength (113 MPa) occurred at 15 wt.%, impact energy (77 J) at 10 wt.%, and hardness (57.2 BHN) also peaked at 10 wt.%. Increasing ash content lowered density, supporting lightweight applications [9].

Friction and wear in reciprocating machinery can be mitigated by the utilization of modern materials and lubrication methods. This research examines the tribological characteristics of aluminum alloy (EN AlSi10Mg) augmented by ferrous-based components, utilizing a ball-on-plate tribometer. Taguchi and artificial neural network models provide ideal parameters, indicating that material composition is the predominant element affecting wear reduction. [10]. AA6083 alloy reinforced with ZrO2 was studied for its mechanical and wear properties using stir casting. The 4% ZrO2 sample showed superior crystallinity, strength, and corrosion resistance, making it ideal for wear applications. SEM and XRD analyses confirmed well-densified microstructures with refined intermetallic phases [11]. The study examines A356 alloy reinforced with different sizes of B4C particles (40 μm and 90 μm) using stir casting. Smaller B4C particles resulted in higher hardness and strength, while both reinforcements slightly reduced ductility. SEM and EDS analyses confirmed uniform distribution of reinforcement within the matrix [12].

Comparative analysis of end milling and ball nose milling of A356/SiC MMC showed that flat end milling achieved higher MRR and minimum SR, indicating its suitability for efficient machining of complex shapes [13]. Turning parameters for A356 aluminum alloy were optimized using response surface methodology (RSM), with depth of cut, spindle speed, and feed rate, refined to achieve optimal SR and MRR, validated through desirability testing [14]. An aluminum A356 metal matrix composite (MMC) reinforced with MoS_2 and wheat husk ash (WHA) was fabricated using a hybridized stir-squeeze casting process. Optimized casting conditions improved tensile strength (TS) by 23.72%, with squeeze pressure effectively reducing porosity and enhancing microstructure [15]. Hybrid dual-phase coatings on A356 aluminum alloy were created using plasma electrolytic oxidation (PEO) and burnishing with MoS_2 and graphite. These coatings showed ultra-low friction (COF as low as 0.02) and high-temperature stability, with lubricious phases forming a protective transfer film under high contact pressures [16]. A356/ Al_2O_3/MoS_2 composites processed by stir casting and extrusion demonstrated enhanced sliding wear resistance, with MoS_2 reducing friction. This secondary processing minimized agglomeration and improved mechanical properties [17].

Squeeze casting was used to fabricate A356/SiC/MoS_2 composites, achieving refined grains and uniform particle distribution at 120 MPa. Increased squeeze pressure reduced wear rates by 46.26% and friction by 41.79% compared to gravity casting, suitable for high-performance applications [18]. Wear tests on A356 nanocomposites reinforced with Al_2O_3 and MoS_2 showed decreased WR and COF as Al_2O_3 and MoS_2 content increased, benefiting tribological properties in applications with variable load and sliding conditions [19]. A356-SiC functionally graded MMC were produced by vertical centrifugal casting, and tribological tests conducted at 350°C indicated that the WR escalated with increasing load. The particle-rich zone exhibited minimum WR and COF related to the matrix-rich zone, where adhesive and metal flow wear dominated [20]. A13Zr/A356 composites were prepared by in-situ reaction with K_2ZrF_6 at varying temperatures, with 750°C showing optimal particle distribution and enhanced wear resistance. At this temperature, friction was higher due to abrasive and oxidation wear modes, while higher temperatures promoted delamination wear [21]. A356 hybrid composites reinforced with $ZrSiO_4$ and TiB_2 showed improved wear resistance under dry sliding due to harder particle reinforcements. The composite with 4% $ZrSiO_4$ and 6% TiB_2 exhibited minimal surface damage and is suitable for aerospace and automotive applications due to its enhanced tribological characteristics [22].

A356/3 wt% Al_3Zr composites synthesized at 750°C showed improved hardness and reduced friction coefficient (0.367) compared to the matrix. The wear mechanism was mainly adhesive with abrasive and fatigue wear, transitioning to delamination wear at higher loads, indicating enhanced wear resistance due to Al_3Zr reinforcement [23]. A356 alloy supplemented with 20 wt% SiC, produced via gravity die casting, stir casting, and squeeze casting, shown enhanced hardness and tensile strength. Squeeze cast samples exhibited the minimum WR and maximal COF under dry sliding conditions, attributed to the superior bonding and load-bearing capacity of SiC particles, while SEM analysis indicated minor adhesive wear and delamination [24]. A356-3 wt% ZrB_2 composites prepared under varying magnetic field frequencies showed improved hardness (up to 235.72 Hv) and reduced wear rates with increased magnetic field frequency. The wear mechanism shifted from adhesive to abrasive wear with higher frequency, enhancing the tribological behavior of the composite [25]. An $Al_5Ti_{0.2}C_{0.2}B_1Ce$ alloy refiner was developed using Al and Ti_6Al_4V chips, containing phases like $TiAl_3$, TiC, and TiB_2. This refiner effectively reduced A356 alloy grain size from 88.9 μm to 38.1 μm, improving its tensile strength by 15.4%, demonstrating resistance to Si poisoning [26].

In this study, EDM factors like I, Ton, and duty cycle were optimized using fuzzy logic and GRA for machining thixoformed A356-5TiB_2 composites. The study revealed significant effects on MRR and surface integrity, evaluated through SEM [27]. The impact of solutionizing temperature and aging time on A356.0 alloy's hardness and tensile strength was investigated. Solutionizing at 540°C, followed by quenching and aging, improved these properties. A pin-on-disc test assessed wear performance, correlating mechanical properties with heat treatment parameters [28]. Research on the use of Wiper geometry in finishing turning of A356, stainless steel, and low alloy steel demonstrated improved surface roughness, especially at higher feed rates. For A356, increasing cutting speed reduced surface roughness by 18%, with stable performance at feed rates above 0.12 mm/rev [29]. A multi-performance optimization study on machining Al/10%SiC PAMMC using RSM highlighted machining time cutting speed, depth of cut and feed rate as key parameters affecting tool flank wear and surface roughness. The numerical model developed was effective for predicting these outcomes [30]. By simulating A356 alloy sand casting, the study used Box-Behnken Design and NSGA-II-TOPSIS optimization to reduce shrinkage volume and solidification time, achieving enhanced casting density and reduced defects. Optimal parameters improved metal fluid flow, reduced solidification time from 129.24 to 88.10s, and shrinkage volume between 9.68 and 4.06 cm^3 [31]. The mechanical and wear performance of A356/Al_2O_3 nanocomposites produced by powder metallurgy showed that increased milling time enhanced hardness and compressive strength but affected wear resistance. Specimens milled for shorter durations demonstrated improved wear performance due to favorable microstructural properties, challenging the conventional hardness-wear correlation [32]. The tribological performance of (Mg_2Si+TiB_2)/A356 composites was studied, revealing that load had the most important effect on WR and COF, followed by TiB_2 content and sliding distance. Optimum wear rate was achieved at

2766 m sliding distance, 3.36 wt% TiB_2 and 26 N load, with SEM and AFM analyses showing improved hardness and surface features due to refined microstructure [33].

While several studies have explored A356-based composites using reinforcements such as SiC, Al2O3, TiB2, and others to enhance mechanical and wear properties, this research uniquely combines Si_3N_4 for structural reinforcement and MoS_2 for lubrication, optimizing both tribological and machining behaviors. A major novelty of this work is the application of used motor oil (UMO) as a sustainable dielectric fluid in EDM, which not only supports eco-friendly manufacturing but also enhances machining performance metrics such as MRR and TWR. Furthermore, this study implements a dual optimization framework using entropy-based weighting and the TOPSIS method to simultaneously optimize wear rate, coefficient of friction, hardness, and EDM characteristics. Unlike prior works, which focus on either tribology or machining separately, this research provides a comprehensive integration of both, including a detailed analysis of MML formation and degradation mechanisms. These advancements make the proposed hybrid composite system especially suitable for high-demand sectors like aerospace and automotive manufacturing.

2. Experimental Methodology

2.1. Preparation of Composites

The A356 alloy defined by the chemical composition in Table 1 was chosen as the matrix material, while silicon nitride (Si_3N_4) and molybdenum sulfide (MoS_2) with a particle size of 25nm were chosen as reinforcements. Before adding the nanoparticles to the melt, which had been heated to 850°C, the alloy was heated to 250°C. The mixture was then mixed at 1000 rpm. A warmed die steel mold of 105 mm × 12 mm was used to poured into the molten liquid, and a flux consisting of 1wt% magnesium powder was added to enhance wettability. In order to remove any surface flaws, the samples were ground to a size of 100 mm length and 10 mm breadth. A hybrid composite was produced using the same approach, incorporating varying MoS_2 weight percentages (0, 2.5, 5, 7.5, and 10 wt%), while maintaining a constant Si_3N_4 of 5wt%. Wear testing under varied loads and sliding velocities indicated the best wear resistance in the Si_3N_4-rich zone, with the minimum wear rate of 0.749×10^{-4} achieved at 20 N, 2 m/s, and 500 m sliding distance. [34].

Table 1. Chemical composition of A356 aluminum alloy [35].

Elements	wt%
Al	Balance
Mn	0.1
Fe	0.2
Zn	0.1
Si	7.5
Mg	0.45
Cu	0.1
Ti	0.2

2.2 Mechanical and Tribological Properties

Scanning electron microscopy (SEM) in conjunction with energy-dispersive X-ray spectroscopy (EDS) mapping was used to examine the homogeneous distribution of composites. The hardness was calculated with respect to ASTM E18-22 standard. The experimental density was determined using the liquid immersion method, and the void fraction was calculated by comparing it to the theoretical density. Genichi Taguchi, the most renowned of this group of Japanese scientists, is renowned for his quality enhancement methods, which are now referred to as the Taguchi method, which use modified fractural DOE [36].Table 2 shows that the wear tests followed ASTM G-99 and that the trials were structured using the Taguchi design of L25 orthogonal array.

Wear rate (WR), surface hardness (HV) and coefficient of friction (COF) were measured as reactions to five different degrees of systematic parameter manipulation involving applied stress, percentage reinforcement, sliding speed, distance, and temperature. Microstructural analysis

showed uniform particle distribution, with improved tensile strength and hardness due to Si_3N_4 and MoS_2 reinforcement with A356 composites. Formula (1) was employed to evaluate the WR, which is displayed in mm^3/min [37]. According to the ASTM E 18-07 standard, the HV was calculated at 10 different spots using hardness equipment. The mean result was recorded as the hardness of the worn surface. Examining the microstructure of the material that had been abraded was done using scanning electron microscopy (SEM).

Table 2. Design of experiments for wear rate

S. No	Factors	Symbols	Unit	Levels				
				1	2	3	4	5
1	Reinforcement	A	wt%	0	2	4	6	8
2	Load	B	N	10	30	50	70	90
3	Sliding Speed	C	m/s	1.1	2.2	3.3	4.4	5.5
4	Sliding distance	D	m	1100	2200	3300	4400	5500
5	Temperature	E	°C	45	90	135	180	225

$$W = \left(\frac{W_b - W_a}{\rho^* t}\right) \tag{1}$$

2.3 EDM of Composites

Research on A356 composites employing UMO as the dielectric fluid was carried out in the following EDM module using the die sink machine. The EDM process known for handling high-strength materials and complex shapes evaluated the machining efficiency with factors like flushing pressure (FP), voltage (V), pulse on-time (Ton), and discharge current (I) were analyzed [38]. Table 3 shows input factors and its levels for EDM process.

Table 3. Electric Discharge machining input factors

S. No	Factors	Notations	Levels				
			1	2	3	4	5
1	Polarity	E	0	2.5	5	7.5	8
2	Concentration of Powder (alumina) (g/l) (wt%)	F	6	12	18	24	90
3	I (A)	G	10	30	50	70	5.5
4	Ton (µs)	H	1.5	2.5	3.5	4.5	5500
5	Gap in Distance (mm)	I	0	2.5	5	7.5	

As a result, the tool wear rate was determined using the MRR, TWR, and Ra measurements. When designing the trials, the Taguchi mixed orthogonal array was utilized. By utilizing equations (2) and (3), the MRR and TWR were calculated [39]. A mean value was taken from ten separate sites where the Mitutoyo roughness tester was used to calculate the Ra value. An SEM analysis was performed on the machined specimen to determine its surface morphology. Parameter modification using TOPSIS technique.

$$MRR = \left(\frac{M_b - M_a}{\rho^* t}\right) \tag{2}$$

$$TWR = \left(\frac{W_b - W_a}{\rho^* t}\right) \tag{3}$$

Where W_b and W_a–Mass of the workpiece before and after the wear test, M_b and M_a– Mass of the workpiece before and after machining, ρ - material density, and t - machining duration in seconds.

2.4 Weight Measurement Using Entropy Technique

The index weight is determined in this study by means of the entropy weight measurement technique. The entropy weight approach uses information amount to determine weights and solves mathematical models independently, without the decision maker's input. The weight index for each machining characteristic is determined using methods that are derived from the research findings.

- Step 1: In the first stage, 'm' alternatives are assessed based on 'n' qualities. In this case, the attributes stand for reaction factors like SR, MRR, ROC, and TWR, and the alternatives are process factors like flushing pressure, pulse on time, and peak current.
- Step 2: The initial findings are transformed into a decision matrix denoted as $D[x_{ij}]_{m\times n}$, whereas m denotes the number of possibilities, n signifies the number of attributes, and x_{ij} denotes the value of the j^{th} attribute for the i^{th} alternative.
- Step 3: For the purpose of comparing the response parameters, the choice matrix is normalized by the maximum values of favorable attributes and the minimum values of non-beneficial attributes. Using the ensuing mathematical equation, it is possible to calculate the normalized matrix.

Lower the Better

$$r_{ij} = \frac{x_{ij} - minimum(x_{ij})}{maximum(x_{ij}) - minimum(x_{ij)}} \tag{4}$$

Higher- the-Better

$$r_{ij} = \frac{maximumx_{ij} - x_{ij}}{maximum(x_{ij}) - minimum(x_{ij})} \tag{5}$$

where $i = 1,2,3 \ldots \ldots mj = 1,2, \ldots . . n$

- Step 4: Subsequent to normalization, substitute the value of r_{ij}. into Equation (5) to determine ' N.

$$N = (r_{ij})_{mmn} \tag{6}$$

Then find $Q = (Q_{ij})_{mun}$

$$Q_{ij} = \frac{r_{ij}}{\sum_{i=1}^{m} r_{ij}} \tag{7}$$

- Step 5: Compute the entropy value e_j which signifies the assessment of the j^{th} index.

$$e_j = -\frac{1}{ln\, m}\sum_{i=1}^{m} Q_{ij}\, ln\, Q_{ij} \tag{8}$$

where $i = 1,2, \ldots . . mj = 1,2, \ldots \ldots n$

- Step 6: Evaluate the entropy weightage (w_j) of the j^{th} index.

$$w_j = \frac{1 - e_j}{n - \sum_{j=1}^{n} e_{ij}} \tag{9}$$

2.5 Ranking the Factors Using TOPSIS Technique

TOPSIS is a mathematical method that integrates the weights of machining parameters according to the decision maker's preferences in order to resolve multi-objective issues and achieve a singular optimal solution. This method is broadly applicable to all suitable practical methods for achieving a viable, faultless solution. The rational approach of the positive and negative ideal solution is characterized by the fact that all experimental results are within the defined limits of maximum and minimum, resulting in satisfactory outcomes.

- Step 1: Normalize the matrix through the subsequent equation.

$$T_{ij} = \frac{x_{ij}}{\sqrt{\sum_{i=1}^{m} x_{ij}^2}} \tag{10}$$

whereas $i = 1,2, \ldots \ldots mj = 1,2, \ldots \ldots nx_{ij}$ denotes the actual value of the i^{th} value of j^{th} experimented run and T_{ij} denotes the corresponded normalized results.

- Step 2: Using the entropy weight measurement method, the weighted matrix for each result is determined.
- Step 3: The weighted normalized decision matrix is produced by multiplying the normalization matrix with the corresponding weights obtained using the entropy weight technique. The following equation is used to find the weighted normalized decision matrix.

$$V_{ij} = w_i \times T_{ij} \tag{11}$$

where $i = 1,2, \ldots \ldots mj = 1,2, \ldots \ldots n, w_j$ denotes the weight of the j^{th} attribute.

- Step 4: The positive ideal solution (V^+), is identified for the optimal value, while the negative ideal solution (V^-) is established for the suboptimal value of each characteristic using the weighted choice matrix as presented below.

$V^+ = (V_1^+, V_2^+, \cdots \cdots V_n^+)$ *Max values*
$V^- = (V_1^-, V_2^-, \cdots \cdots V_n^-)$Min values

- Step 5: The subsequent equation is employed to determine the separation distance of each viable solution from the V^+ (S+) and the V^- (S−).

$$S_i^+ = \sqrt{\sum_{j=1}^{n} (V_{ij} - V_J^+)^2} \tag{12}$$

$$S_i^- = \sqrt{\sum_{j=1}^{n} (V_{ij} - V_J^-)^2} \tag{13}$$

whereas $i = 1,2, \ldots \ldots mj = 1,2, \ldots \ldots n$

- Step 6: The equation is used to evaluate the relative closeness coefficient, CCo, to the ideal solution [40].

$$CC_o = \frac{S_i^-}{S_t^+ + S_i^-} \tag{14}$$

- Step 7: Ranking the order.

The closeness-coefficient value is used to organize a collection of alternative data in ascending order.

3. Results and Discussion

3.1 Results on Wear Behavior of Hybridized Composites

The microstructure of the composites is illustrated in figure 1, showing uniform particle dispersion. The matrix material was uniformly distributed, with reinforcements depicted in black and each element displayed in a unique type. The hardness of the composites rises up to a 2.5 wt% of MoS_2 content, and thereafter it drops due to the inverse effect of Hall-Petch and an improve in the porosity percentage; is indicate in Fig 2.

The granule particles are refined by the incorporation of flux, which leads to a decrease in hardness. This phenomenon has been observed by other researchers. Materials demonstrate increased

softness when their particle size decreases below a specific threshold, as indicated by the inverse Hall-Petch relationship.

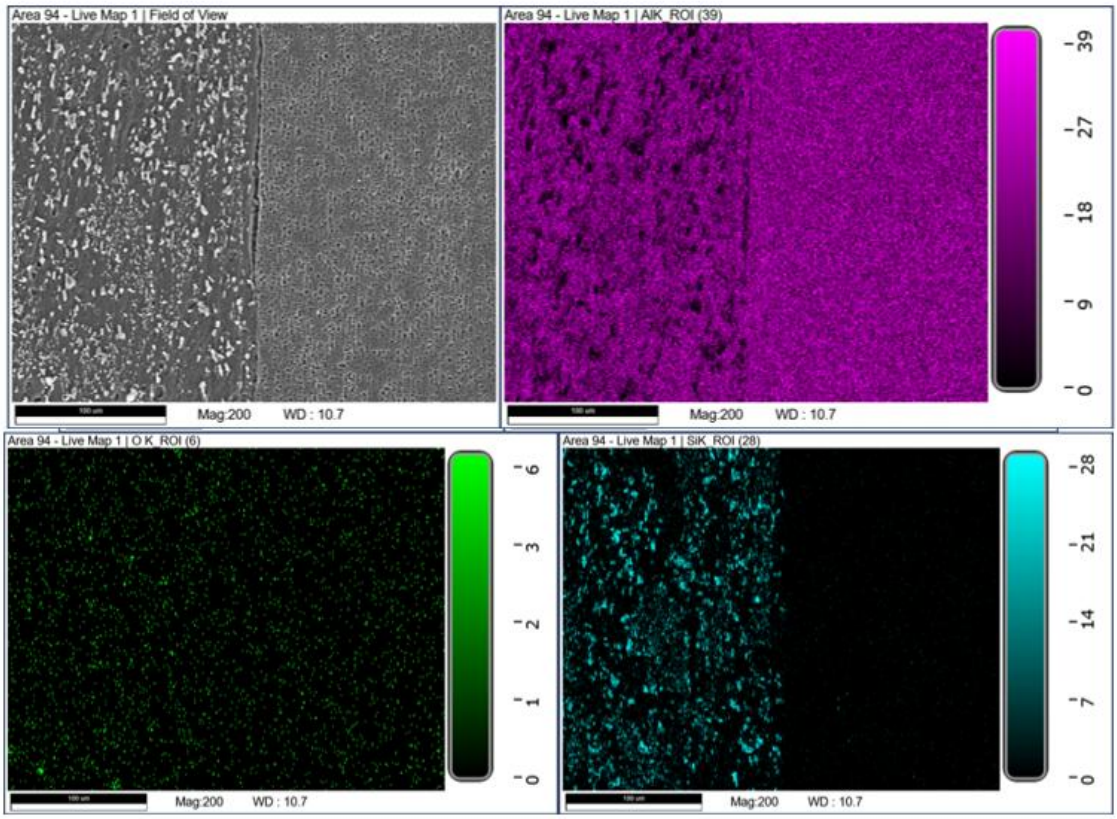

Fig. 1. Analysis of SEM with EDAX of A356 hybridized composites

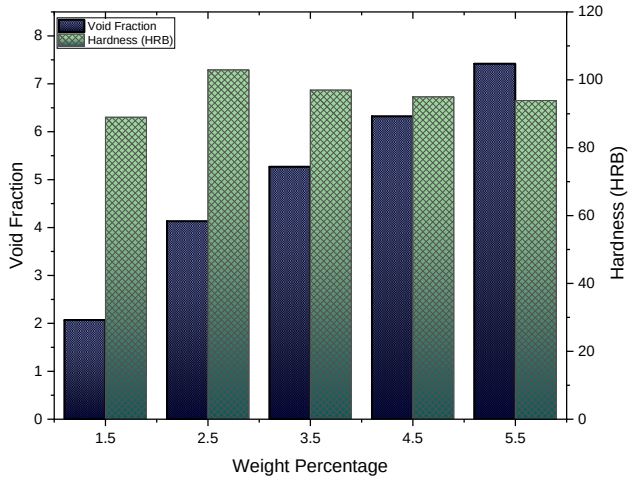

Fig. 2. Evaluation of Hardness of A356 hybrid composites at various MoS_2 percentage

Figure 3 shows how various process factors affect the process of composite deterioration. Adding 2.5% MoS_2 particles to the matrix material increases its wear resistance, as shown in the graph. The EDAX investigation illustrated in figure 4 demonstrates that the insertion of particles results in the removal of material from the contact surface during sliding, which leads to the formation of an mechanically mixed layer (MML) and third body attrition.

The maximum wear rate of 0.00771 mm^3/min was achieved for MoS_2 (10 wt%) when the particle content reaches at 2 wt%. The WR rises as the temperature increases, as evidenced by the trend line, which recorded a highest WR of 0.0086 mm^3/min at 225°C. Upon attaining plastic deformation at elevated temperatures, aluminum experiences a loss of hardness. The dislodged reinforced

particles degraded the composite pin's substance as a result of other-body wear. At 70N, the WR steadily surges until it reaches the peak point, at which point it decreases. The direct contact that occurs when the contacting surface applies significant pressure under increased load resulting in the degradation of the MML, which is the cause of the elevated attrition rate.

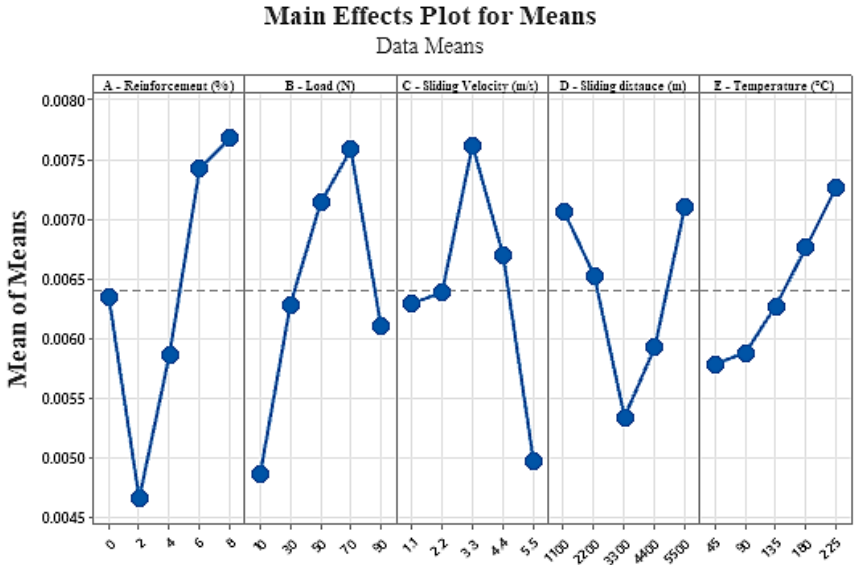

Fig. 3. Main effect plot for wear rate

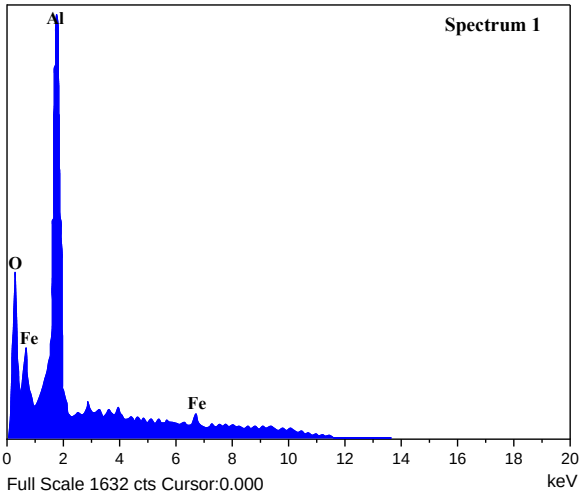

Fig. 4. EDAX morphology of the worn surface

At a load of 45N, the wear rate transitioned from moderate to high, indicating that the composites produced remained stable as high as 50N. The attrition rate increased until 3.3 m/s at which point it decreased, and the sliding velocity followed a similar pattern. As determined by a thermocouple, the composite pin reaches a temperature of 469°C when exposed to temperatures exceeding 180°C under conditions of elevated load and sliding speedz`. It is confirmed by the presence of oxygen in the EDAX analysis that this condition leads to the production of a tribo-rich oxidation layer. Over prolonged sliding distances, the pin's surface undergoes substantial deformation and a rapid increase in temperature. The MML was segmented according to the distance increment, which led to delamination wear. EDAX analysis (Figure 4) confirmed third-body debris and iron transfer, indicating MML formation, which reduced wear by acting as a protective layer. The friction behavior of A356 hybrid composites was 0.438 with the addition of 2% MoS_2 particles, 0.221 with 6% MoS_2 particles, and 0.225 for unreinforced composites, as illustrated in Fig 5.

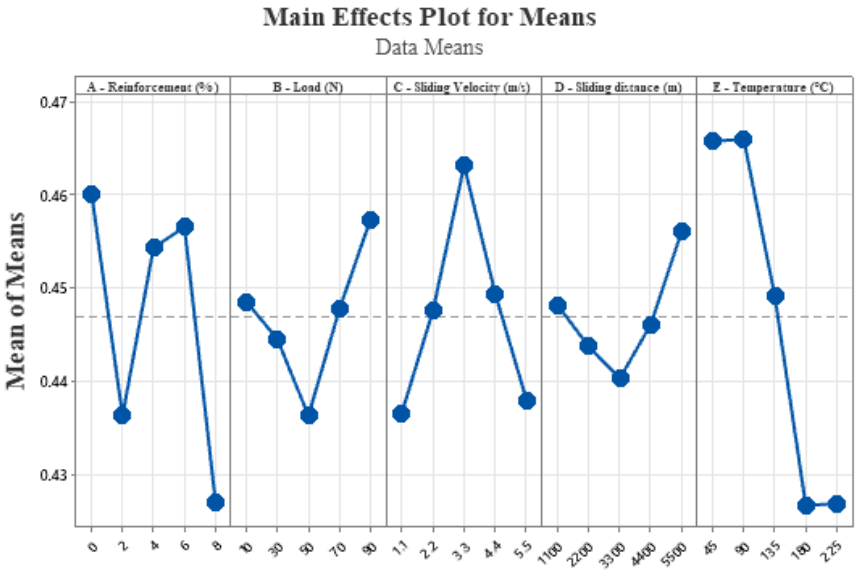

Fig. 5. Main effect plot of coefficient of friction of hybridized composites

The addition of MoS_2 was found to result in a decrease in the coefficient of friction (COF) due to the production of an MML at the surface. The results denotes that the most effective MML was produced at a concentration of 2 wt%, which subsequently led to the minimum wear rate. This finding was also consistent with the experimented data. The MML layer experiences failure at factor of 50 N for load and 3300 m for sliding distance, suggesting that the wear rate transitions from minimum to maximum beyond these thresholds. Materials achieve a plastic state at high temperatures and velocities, which results in a decrease in hardness and a decrease in the coefficient of friction (COF). Temperature is the most significant factor influencing the hardness of the worn surface, as plain from Figure 6. The following factors were identified as contributing to the increase in surface hardness. (i) Recrystallization occurs when the composite pin reaches a temperature of 469°C; further investigation is required. (ii) The EDAX mapping clearly demonstrates the transmission of iron from the counter-face.

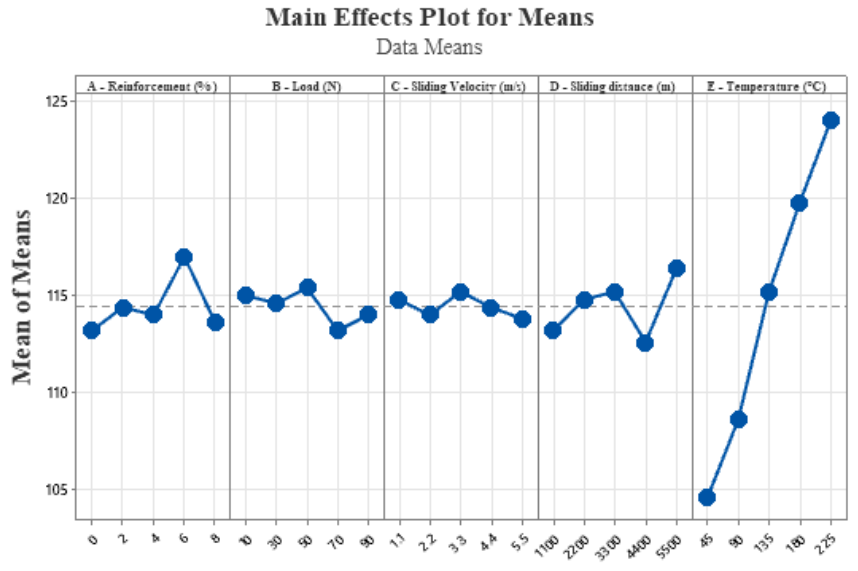

Fig. 6. Main effect plot of the HRB of hybridized composites

Fig 7(a) illustrates the deteriorated surface morphology of the pin that was machined at 180°C. The worn surface was evidently marked by fissures and pits. The fracture originates in a different zone and culminates in the pit, and it was referred to as a Type 1 crack. Ploughing erosion was indicated by the materials' tendency to migrate toward the surface rather than being removed from it. The elevated temperatures caused some of the materials to deform and resolidify on the surface. As

illustrated in Figure 7(b), the plastic flow was apparent at a magnification of 1.00kx, confirming that the material has reached its deformation temperature. The pits are dispersed throughout the surface and have a dimension that ranges from 1 µm to 5 µm. It was classified as a type 2 crack when a micro crack of 5–6 µm was observed on slides at a temperature of 50 °C. The crack had a distinct beginning and ending point. SEM analysis showed smoother worn surfaces in chilled samples, confirming improved tribological properties [41].

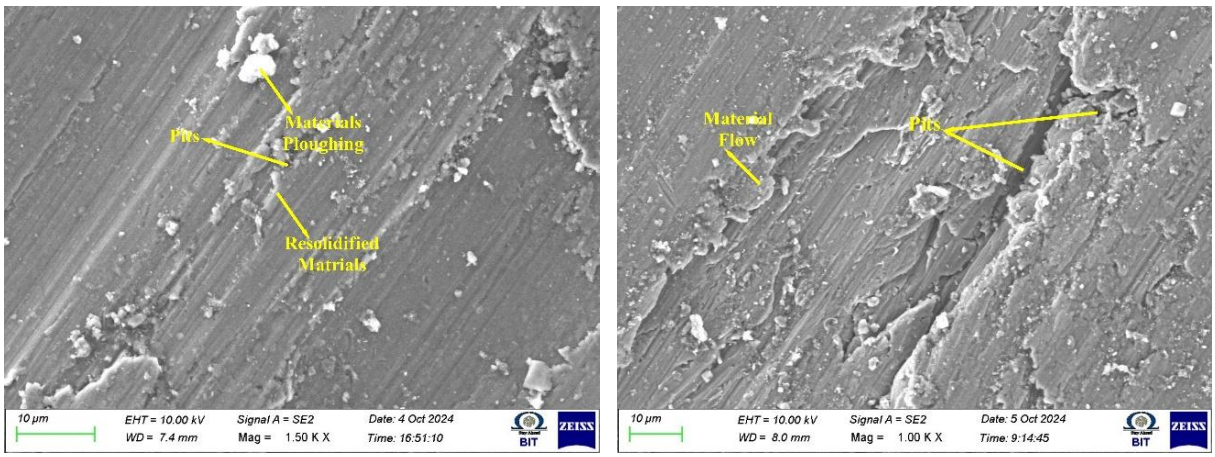

(a) (b)

Fig. 7. SEM image of WR of A356 hybridized composites at 180°C: (a) at 1.50kx magnification, (b) at 1.00kx magnification

Figure 8(a) illustrates the distinct observability of the resolidified materials and the increased quantity of microscopic fissures on the surface. Micro fissures measuring 0.25µm to 0.5µm were clearly visible at 2.00kx. The mode of wear was identified as adhesive, and the plasticization of materials occurred, as illustrated in figure 8(b). Figure 9(a) plainly illustrates that cracks originated at multiple locations and converged at a single spot at a temperature of 180 °C, qualifying as type 3 cracks. Direct contact is the consequence of the mechanically mixed layer and protective layers failing, which establishes a pathway for delaminated wear. Figure 9(b) illustrates that material ploughing, micro fissures, and fractures were evident at a magnification of 500x.

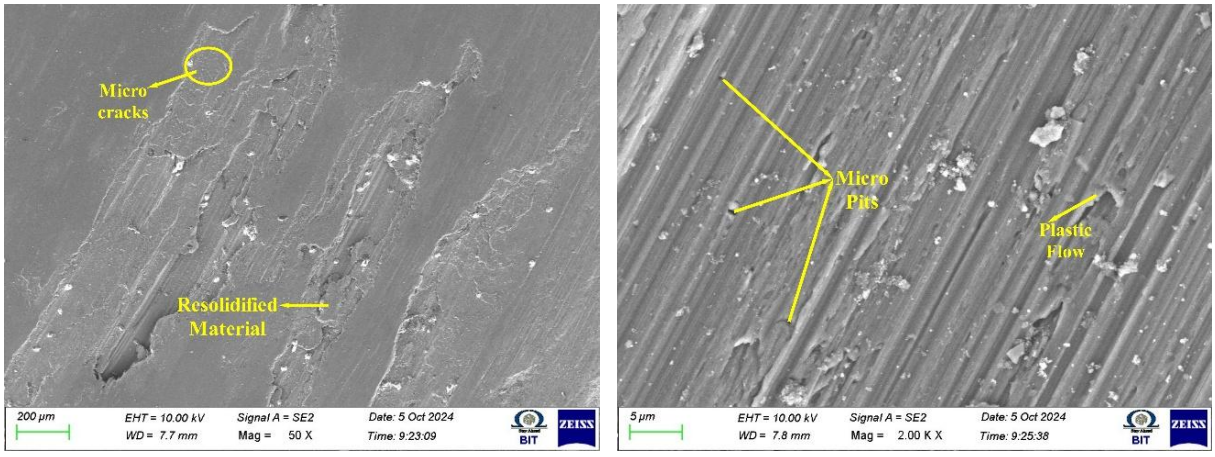

(a) (b)

Fig. 8. SEM image of Wear rate of A356 hybridized composites slides at 45°C at (a) 50x (b) 2.00kx

SEM images at 180°C and 225°C (Figures 7 and 9) revealed microcracks, pits, and layered material removal, confirming delamination wear at higher loads and temperatures. The MML improved wear resistance initially, but its instability under extreme conditions led to delamination failure, accelerating material degradation. The final phase consisted of the identification of the optimal

alternative from the available alternatives. This was achieved by conducting 25 experiments and measuring three responses, as shown in Table 4.

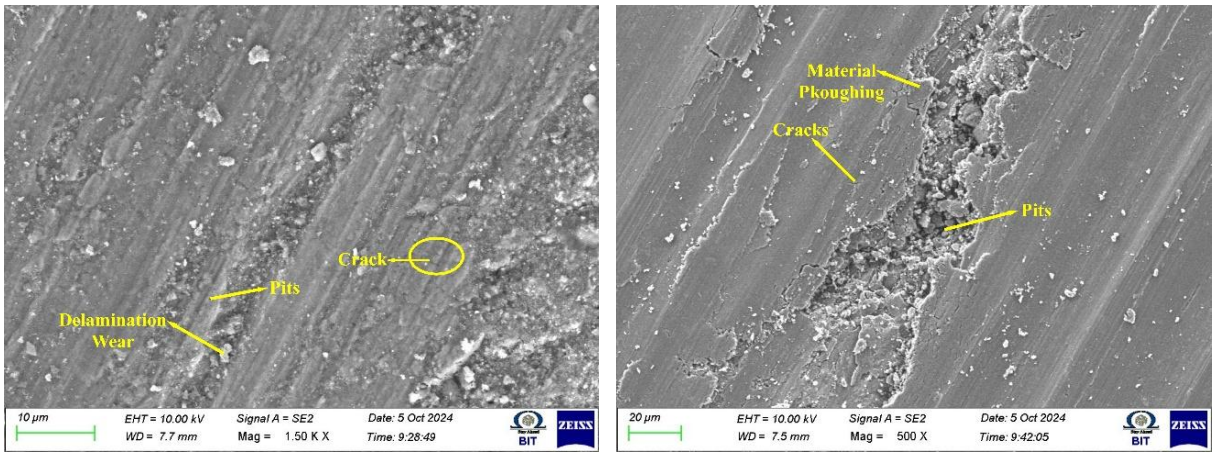

(a) (b)

Fig. 9. SEM image of Wear rate of A356 hybridized composites slides at 225 °C at (a) 1.50kx (b) 500x

Table 4. Design of experiments with inputs and its results

S.No	A(wt%)	B (N)	C (m/s)	D (m)	E (C)	WR (mg/ min)	COF	Hardness on Worn surface (HRB)
1	0	10	1.1	1100	45	0.00546	0.482	103
2	0	30	2.2	2200	90	0.00607	0.479	109
3	0	50	3.3	3300	135	0.00771	0.464	116
4	0	70	4.4	4400	180	0.00809	0.438	115
5	0	90	5.5	5500	225	0.00439	0.438	123
6	2	10	2.2	3300	180	0.00061	0.399	120
7	2	30	3.3	4400	225	0.00687	0.440	123
8	2	50	4.4	5500	45	0.00604	0.461	109
9	2	70	5.5	1100	90	0.00515	0.451	105
10	2	90	1.1	2200	135	0.00463	0.431	115
11	4	10	3.3	5500	90	0.00611	0.496	111
12	4	30	4.4	1100	135	0.00479	0.445	113
13	4	50	5.5	2200	180	0.00637	0.422	120
14	4	70	1.1	3300	225	0.00700	0.423	125
15	4	90	2.2	4400	45	0.00506	0.486	101
16	6	10	4.4	2200	225	0.00778	0.440	127
17	6	30	5.5	3300	45	0.00458	0.453	107
18	6	50	1.1	4400	90	0.00527	0.441	110
19	6	70	2.2	5500	135	0.00989	0.480	118
20	6	90	3.3	1100	180	0.00963	0.469	123
21	8	10	5.5	4400	135	0.00435	0.426	114
22	8	30	1.1	5500	180	0.00912	0.406	121
23	8	50	2.2	1100	225	0.01031	0.394	122
24	8	70	3.3	2200	45	0.00780	0.447	103
25	8	90	4.4	3300	90	0.00682	0.463	108
					Wij	0.942	0.026	0.032

The composites can endure a A of 60N, B of 2.2 m/s, C of 5500 m, and D of 180°C, as demonstrated by the sixth testing session, which also displayed the greatest total value in Table 5. According to Table 5, Experiment No. 6 has the maximum closeness coefficient value of 0.8591. Consequently, the most optimal process parameters for this machining behavior during the EDM method are represented by experiment No. 6. 2% reinforcement, 10 N Load, 2.2 m/s velocity, 3300 m distance, and 180°C temperature are the optimal process parameters for trial 6. The respective values for MRR, COF, and worn surface hardness are 0.00061 mg/min, 0.399 μ, and 120 HV. The composite A356/6Si_3N_4/2MoS_2 demonstrated superior performance, capable of withstanding loads up to 70N and operating at temperatures up to 135 °C. Both GRA and TOPSIS confirmed optimal tribological characteristics at 40 N load, 1 m/s speed, and 3 wt% Gr, with A356 composites with adhesive and delamination wear observed on worn surfaces [42].

Table 5. Determination of the TOPSIS ranking for wear analysis

	Normalization			Weight			Dj+	Dj-	Pi*	Rank
S.No	WR	COF	Hardness	WR	COF	Hardness				
1	0.0193	0.2039	2.7233	0.0182	0.0053	0.0871	0.0260	0.0162	0.3849	17
2	0.0215	0.2026	2.8819	0.0202	0.0053	0.0922	0.0237	0.0157	0.3975	15
3	0.0273	0.1963	3.0670	0.0257	0.0051	0.0981	0.0254	0.0154	0.3767	20
4	0.0286	0.1853	3.0406	0.0270	0.0048	0.0973	0.0269	0.0140	0.3419	22
5	0.0155	0.1853	3.2521	0.0146	0.0048	0.1041	0.0130	0.0271	0.6752	2
6	0.0022	0.1688	3.1728	0.0020	0.0044	0.1015	0.0059	0.0361	0.8591	1
7	0.0243	0.1862	3.2521	0.0229	0.0048	0.1041	0.0211	0.0219	0.5085	7
8	0.0214	0.1950	2.8819	0.0201	0.0051	0.0922	0.0237	0.0158	0.3998	14
9	0.0182	0.1908	2.7762	0.0172	0.0050	0.0888	0.0240	0.0175	0.4222	12
10	0.0164	0.1823	3.0406	0.0154	0.0047	0.0973	0.0168	0.0223	0.5706	4
11	0.0216	0.2098	2.9348	0.0204	0.0055	0.0939	0.0228	0.0164	0.4175	13
12	0.0169	0.1883	2.9877	0.0160	0.0049	0.0956	0.0183	0.0210	0.5346	5
13	0.0225	0.1785	3.1728	0.0212	0.0046	0.1015	0.0201	0.0208	0.5084	8
14	0.0248	0.1790	3.3050	0.0233	0.0047	0.1058	0.0214	0.0231	0.5198	6
15	0.0179	0.2056	2.6704	0.0169	0.0053	0.0855	0.0265	0.0175	0.3972	16
16	0.0275	0.1862	3.3578	0.0259	0.0048	0.1075	0.0239	0.0236	0.4966	9
17	0.0162	0.1917	2.8290	0.0153	0.0050	0.0905	0.0215	0.0198	0.4791	10
18	0.0186	0.1866	2.9084	0.0176	0.0049	0.0931	0.0212	0.0184	0.4656	11
19	0.0350	0.2031	3.1199	0.0329	0.0053	0.0998	0.0319	0.0145	0.3121	24
20	0.0341	0.1984	3.2521	0.0321	0.0052	0.1041	0.0303	0.0188	0.3827	18
21	0.0154	0.1802	3.0141	0.0145	0.0047	0.0965	0.0166	0.0227	0.5774	3
22	0.0323	0.1718	3.1992	0.0304	0.0045	0.1024	0.0288	0.0174	0.3767	19
23	0.0365	0.1667	3.2256	0.0343	0.0043	0.1032	0.0326	0.0178	0.3533	21
24	0.0276	0.1891	2.7233	0.0260	0.0049	0.0871	0.0314	0.0085	0.2139	25
25	0.0241	0.1959	2.8555	0.0227	0.0051	0.0914	0.0262	0.0131	0.3325	23
			A+	0.0020	0.0043	0.1075				
			A-	0.0343	0.0055	0.0855				

3.2 Electric Discharge Machining of Composites

This study aimed to employ used motor oil (UMO) as the dielectric fluid to achieve value from waste. The viability of UMO as a dielectric fluid was assessed by comparing its characteristics with those of standard dielectric fluids. The UMO density is 900 kg/m^3, facilitating improved flushing, while a breakdown strength of 63 kV leads to an extended machining cycle. The machined surface shows black areas, which could be explained by the carbon percentage, which varies between 91% and 94%. The increased heat transfer and dissipation are made possible by the 2.3 mm^2/s kinematic viscosity and the thermal conductivity of 0.136 W/m·K. Table 6 shows the properties of UMO.

Table 6. Characteristics of the UMO

Factors	UMO	EDM oil	Benefits
Kinematic Viscosity at 40°C	2.3mm^2/s	2.13mm^2/s	Low viscosity accelerates heat transmission, rendering it an unfavorable condition.
Density	900kgm^{-3}	813Kg/m^3	Higher density facilitates flushing.
Carbon Content	94%–96%	91%	Oil with elevated carbon concentration results in black spots on the machined surface.
Dielectric Strength	60KVA	45KVA	Machining productivity is enhanced by higher dielectric strength.
Flash Point	221°C	109°C	An enhanced flash point enhances worker safety.
Thermal Conductivity	0.136 W mk^{-1}	0.120W mk^{-1}	Enhanced thermal conductivity accelerates the rate of heat dissipation.
Color	Black	Colorless	Adverse situation: sample is not visible.
Specific Heat	1.693KJ/KgK	2.142KJ/KgK	Minimum specific heat is not an optimal condition.

Due to matrix particulates that induce substantial wear and degrade surface quality, machining composites is a formidable challenge. To avoid stirring the materials directly, the EDM machining technique involved dissolving and vaporizing them to harness the spark's heat. Figure 10 illustrates that the composites demonstrated a 28.5% increase in MRR when associated with the positive polarity. The cathode-linked materials absorbed the mainstream of the heat generated during the spark cycle, prompting numerous other researchers to report comparable findings. According to the findings, the material removal rate (MRR) in the unmixed UMO medium was 0.20 mm^3/min. The rate improved to 0.28 mm^3/min upon the introduction of 5 g/*l* of alumina particles into the dielectric fluid.

Fig. 10. Main effect plot of MRR of hybridized composites.

Particles that pass in the sparkle gap and travel in a crisscross shape among the tool and rod are believed to be responsible for the bridging action that increases heat and, consequently, MRR. The MRR dropped because the machined debris became denser after being mixed with 7.5 g/*l* of alumina in the dielectric fluid. According to the experimental results, the increased current creates a high-intensity discharge, which leads to a greater amount of heat and, as a result, the removal of a greater amount of material from the workpiece. The MRR decreases as a result of the plasma channel's expansion at elevated parametric current levels. The MRR was pointedly improved by a surge in the Ton, which was the duration for which the spark was maintained within the machined gap. The material removal rate (MRR) decreases as a result of insufficient cleansing when the parametric level exceeds 45 μs, as a substantial volume of material has been extracted from the

surface. An increase in gap distance leads to a reduction in heat intensity and a decrease in MRR as the distance between the electrodes increases.

Fig. 11. Influence of various factor on TWR of hybridized composites.

The TWR was reduced and a high MRR was achieved by utilizing copper as the tool material in this endeavor, thereby increasing productivity in the EDM sector. With the electrodes connected in a positive polarity, as shown in Figure 11, the TWR was low, suggesting that most of the heat was transferred to the workpiece. The reduction in spark distance caused by the bridge effect causes the TWR to drop up 5 g/*l* concentrations. This causes the spark gap to slightly widen in order to keep the spark distance constant, which in turn reduces the TWR and heat intensity. When the current or Ton increases, the TWR rises owing to the development of a plasma channel maximum intensity. The Tool wear rate decreases as the separation distance rises till it attains the peak point of 3.5 mm, at which point it increases. Machining A356-TiB_2 nanocomposites via EDM revealed challenges like thermal degradation and erosion. Control parameters, including pulse current and duty cycle, influenced surface roughness and MRR, impacting quality and productivity, making these composites suitable for high-performance applications [43].

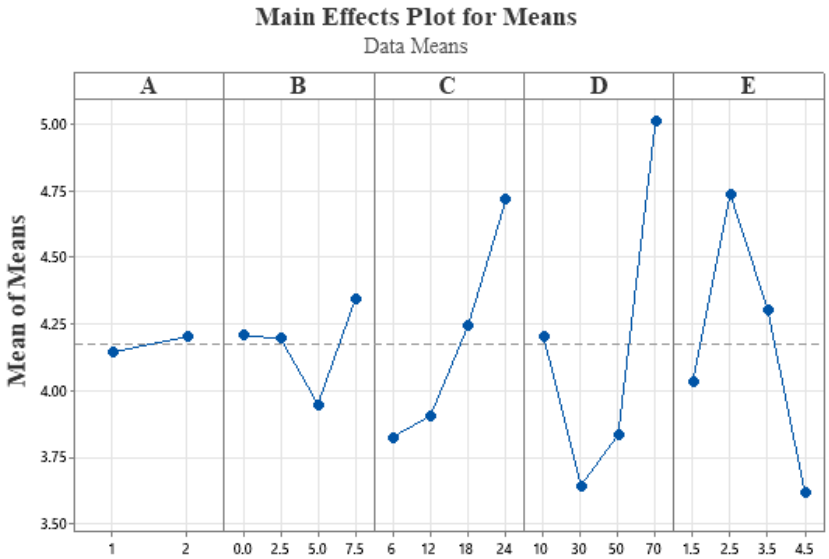

Fig. 12. Impact of various factor on Surface roughness (Ra) on the hybridized composites.

Figure 12 illustrates that the Ra values of the composites are minimally affected by polarity, as evidenced by the Ra values of 4.146 μm and 4.203 μm for the positive and negative polarities,

respectively. A strong spark produced by an increase in current degrades surface quality by making craters and tiny holes. The integration of 2.5 g/*l* of Alumina particles has no effect on Ra, whereas a concentration of 5 g/*l* achieves the least Ra of 3.951 µm. The bridging effect resulted in the comprehensive removal of machining debris, which in turn improved the surface quality. The mean Ra was 3.828 µm at a parametric Ton of 30 µs. Nevertheless, the average Ra markedly rise to 4.715 µm when the Ton was elevated to 70 µs. Densifying the plasma channel allowed a remelted surface layer to emerge, which was thought to be responsible for the rise. As the gap distance increases, the surface quality improves because the machined debris is completely eliminated, preventing the creation of void and a delamination layer.

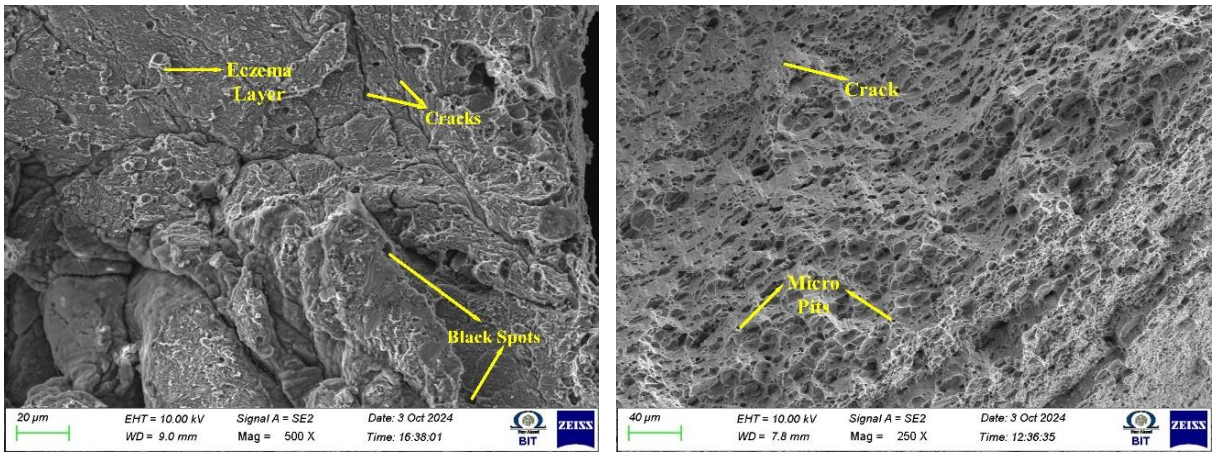

(a) (b)

Fig. 13. SEM image of EDM machined surface of A356 hybridized composites produced with clean UMO: (a) at 1.00kx magnification; (b) at 250x magnification

Figure 13(a) illustrates the machined surface morphology of A356 hybridized composites that were processed with purified used motor oil. The dielectric fluid deposited on the surface was found to contain carbon content, as evidenced by the black specks that were visible throughout the morphology. The intense heat generated by the explosion resulted in the formation of craters on the surface. The unequal distribution of heat made the layer easily discernible on the surface morphology. Resolidified substances were plainly noticeable at a 250X n, as indicate in fig 13(b), indicating that the machining debris had not been adequately removed. Figure 14(a) demonstrates that black areas and crust were distinctly observable on the surface during the machining of the UMO dielectric medium containing 6 g/*l* Alumina.

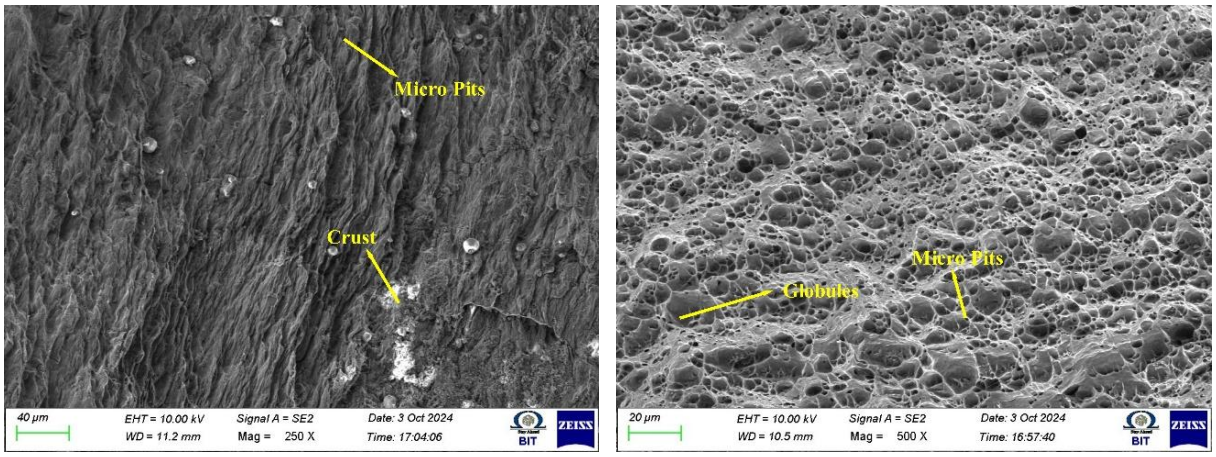

(a) (b)

Fig. 14. SEM image of EDM machined surface of A356 hybridized composites produced with UMO and 6% Alumina: (a) at 250x magnification, (b) at 500x magnification.

The heat generated was variably distributed throughout the surface, as evidenced by the distinct appearance of the crust and trough. As illustrated in fig 14(b), globules ranging between 6 µm and 12 µm were evidently at high magnification. This situation was further intensified by the inadequate blushing of machining refuse. Other surface abnormalities discovered included micro pits and micro fractures, which contribute to the degradation of Ra. The dielectric medium, which contained 5 g/*l* alumina particles, was observed to have micro fissures and craters on its surface, shown in fig 15(a). As a result of the increased kinematic viscosity, the machining cycle occurred more frequently, which made it difficult to achieve uniform distribution.

Table 7. Experimental outcomes of EDM

S.No	E	F (g/*l*)	G (A)	H (µs)	I (mm)	Surface Roughness (µm)	MRR (mm^3/ min)	TWR (mm^3/ min)
1	1	0.0	6	10	1.5	3.899	0.4550	0.0682
2	1	0.0	12	30	2.5	3.608	0.2420	0.3011
3	1	0.0	18	50	3.5	6.061	0.0635	0.2863
4	1	0.0	24	70	4.5	4.271	0.6892	0.3251
5	1	2.5	6	10	2.5	3.640	0.3060	0.1593
6	1	2.5	12	30	1.5	3.253	0.2530	0.1351
7	1	2.5	18	50	4.5	3.002	0.6490	0.3310
8	1	2.5	24	70	3.5	4.288	0.3042	0.2123
9	1	5.0	6	30	3.5	3.246	0.3262	0.0829
10	1	5.0	12	10	4.5	5.098	0.3998	0.1767
11	1	5.0	18	70	1.5	3.367	0.5491	0.3387
12	1	5.0	24	50	2.5	2.383	0.4464	0.0996
13	1	7.5	6	30	4.5	3.102	0.4578	0.1101
14	1	7.5	12	10	3.5	2.876	0.3584	0.1598
15	1	7.5	18	70	2.5	8.083	0.2824	0.1855
16	1	7.5	24	50	1.5	6.152	0.5688	0.1945
17	2	0.0	6	70	1.5	5.898	0.2954	0.4944
18	2	0.0	12	50	2.5	3.445	0.2515	0.2030
19	2	0.0	18	30	3.5	3.353	0.3109	0.2313
20	2	0.0	24	10	4.5	3.127	0.1494	0.2926
21	2	2.5	6	70	2.5	5.157	0.2899	0.1711
22	2	2.5	12	50	1.5	3.964	0.5558	0.2458
23	2	2.5	18	30	4.5	2.690	0.3117	0.2051
24	2	2.5	24	10	3.5	7.578	0.1144	0.2219
25	2	5.0	6	50	3.5	3.253	0.3467	0.0386
26	2	5.0	12	70	4.5	5.231	0.3645	0.1505
27	2	5.0	18	10	1.5	2.432	0.1571	0.2676
28	2	5.0	24	30	2.5	6.593	0.4364	0.1625
29	2	7.5	6	50	4.5	2.429	0.2114	0.2351
30	2	7.5	12	70	3.5	3.789	0.1877	0.1706
31	2	7.5	18	10	2.5	4.983	0.6771	0.2454
32	2	7.5	24	30	1.5	3.330	0.3465	0.2024
					Wj	0.229	0.398	0.373

Upon further magnification, as illustrated in figure 15(b), the morphology is observed to contain globules, a remelted layer, micro pits, and micro fractures. According to Table 8, Experiment No. 12 exhibits the maximum closeness coefficient value of 0.8174. As a result, experiment No. 12 comprises the most optimal process parameters for this machining behavior through the EDM process of this study. The ideal processing factors were polarity 1, concentration of alumina 5 g/l, current 24 A, Ton 50 µs, and distance gap 2.5 mm. The related responses are MRR 0.4464 mm^3/min, TWR 0.0996 mm^3/min, and surface roughness 2.383 µm. Table 7 shows the experimental input

and its outcome of this study. Table 8 shows the TOSIS evaluation of ranking analysis of EDM process.

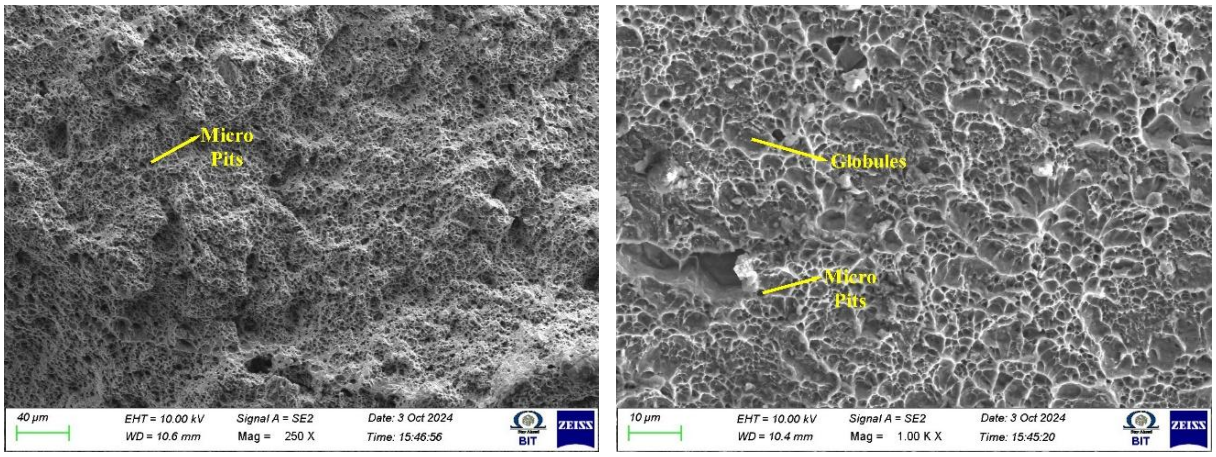

(a) (b)

Fig. 15. SEM image of EDM surface of A356 hybridized composites with 4% MoS_2 with used motor oil at: (a) 250x, (b) 1.00kx

Table 8. Experimental outcomes of EDM

	Normalization			Weight						
S. No	WR	COF	Hardness	WR	COF	Hardness	Dj+	Dj-	Pi*	Rank
1	0.1909	0.0372	0.4771	0.0760	0.0139	0.1092	0.0580	0.1599	0.7336	4
2	0.1016	0.1645	0.4415	0.0404	0.0613	0.1011	0.0981	0.1347	0.5788	22
3	0.0267	0.1564	0.7417	0.0106	0.0583	0.1698	0.1552	0.0707	0.3131	30
4	0.2892	0.1776	0.5226	0.1151	0.0662	0.1197	0.0788	0.1533	0.6606	13
5	0.1284	0.0870	0.4454	0.0511	0.0325	0.1020	0.0771	0.1476	0.6570	14
6	0.1062	0.0738	0.3980	0.0423	0.0275	0.0911	0.0793	0.1571	0.6646	12
7	0.2723	0.1808	0.3673	0.1084	0.0674	0.0841	0.0624	0.1759	0.7382	3
8	0.1277	0.1159	0.5247	0.0508	0.0432	0.1202	0.0907	0.1274	0.5840	21
9	0.1369	0.0453	0.3972	0.0545	0.0169	0.0910	0.0659	0.1653	0.7150	7
10	0.1678	0.0965	0.6238	0.0668	0.0360	0.1429	0.0944	0.1197	0.5591	24
11	0.2304	0.1850	0.4120	0.0917	0.0690	0.0943	0.0710	0.1583	0.6902	10
12	0.1873	0.0544	0.2916	0.0746	0.0203	0.0668	0.0424	0.1899	0.8174	1
13	0.1921	0.0601	0.3795	0.0765	0.0224	0.0869	0.0459	0.1730	0.7902	2
14	0.1504	0.0873	0.3519	0.0599	0.0326	0.0806	0.0621	0.1684	0.7307	6
15	0.1185	0.1013	0.9890	0.0472	0.0378	0.2265	0.1761	0.0728	0.2924	31
16	0.2387	0.1062	0.7528	0.0950	0.0396	0.1724	0.1121	0.1174	0.5115	27
17	0.1240	0.2700	0.7217	0.0493	0.1007	0.1653	0.1505	0.0724	0.3249	29
18	0.1055	0.1109	0.4215	0.0420	0.0414	0.0965	0.0857	0.1463	0.6305	18
19	0.1305	0.1263	0.4102	0.0519	0.0471	0.0939	0.0792	0.1488	0.6527	16
20	0.0627	0.1598	0.3826	0.0249	0.0596	0.0876	0.1060	0.1455	0.5785	23
21	0.1216	0.0935	0.6310	0.0484	0.0349	0.1445	0.1059	0.1117	0.5134	26
22	0.2333	0.1342	0.4851	0.0928	0.0501	0.1111	0.0651	0.1505	0.6980	9
23	0.1308	0.1120	0.3292	0.0521	0.0418	0.0754	0.0721	0.1674	0.6989	8
24	0.0480	0.1212	0.9272	0.0191	0.0452	0.2123	0.1783	0.0579	0.2451	32
25	0.1455	0.0211	0.3981	0.0579	0.0079	0.0912	0.0622	0.1708	0.7331	5
26	0.1530	0.0822	0.6401	0.0609	0.0307	0.1466	0.0991	0.1176	0.5425	25
27	0.0659	0.1462	0.2975	0.0262	0.0545	0.0681	0.1004	0.1657	0.6227	19
28	0.1831	0.0887	0.8068	0.0729	0.0331	0.1847	0.1278	0.1010	0.4413	28
29	0.0887	0.1284	0.2972	0.0353	0.0479	0.0681	0.0893	0.1688	0.6541	15
30	0.0788	0.0932	0.4636	0.0314	0.0348	0.1062	0.0964	0.1388	0.5901	20

31	0.2841	0.1341	0.6097	0.1131	0.0500	0.1396	0.0842	0.1436	0.6305	17
32	0.1454	0.1105	0.4075	0.0579	0.0412	0.0933	0.0714	0.1533	0.6824	11
			A+	0.1151	0.0079	0.0668				
			A-	0.0106	0.1007	0.2265				

4. Conclusions

This research investigates the fabrication and performance characteristics of A356 aluminum matrix hybrid composites reinforced with silicon nitride (Si_3N_4) and molybdenum disulfide (MoS_2), produced through the stir casting method. The study demonstrates that these hybrid composites exhibit significantly improved tribological and machining behavior when compared to conventional A356-based composites reinforced with particles such as silicon carbide (SiC), aluminum oxide (Al_2O_3), titanium diboride (TiB_2), and zirconium silicate ($ZrSiO_4$). Notably, the composite containing 2 wt% MoS_2 delivered the best tribological performance, achieving the lowest wear rate of 0.00061 mg/min and a coefficient of friction of 0.399. This enhancement is primarily attributed to the formation of a stable mechanically mixed layer (MML) on the wear surface. The MML acts as a solid lubricant, reducing direct contact between surfaces, thereby minimizing both friction and material loss. However, at elevated operating conditions—specifically at 225°C under a load of 70 N—the MML begins to degrade, leading to delamination wear. This form of wear involves the formation and propagation of surface cracks, resulting in the peeling or flaking of material, which accelerates component degradation. The highest hardness observed in the study was 127 HRB with the inclusion of 6 wt% MoS_2, surpassing the hardness of typical A356/Si_3N_4 composites (~110 HRB). This increase in hardness is attributed to finer microstructural grains and a more uniform reinforcement distribution. Nonetheless, further increase in MoS_2 content led to porosity and agglomeration of particles, negatively impacting the composite's mechanical integrity. In terms of machinability, electrical discharge machining (EDM) tests revealed that the optimum surface roughness (Ra = 2.383 µm) was achieved using a dielectric fluid containing 5 g/L alumina, with a discharge current of 24 A and a pulse on-time of 50 µs. Additionally, using used motor oil (UMO) as an alternative dielectric fluid improved both the material removal rate (MRR) and tool wear rate (TWR), offering an environmentally sustainable option. However, an alumina concentration of 7.5 g/L resulted in a rougher surface finish (Ra = 8.083 µm), likely due to excessive particle accumulation disrupting the spark stability. These advanced composites are ideal for high-demand applications in automotive, aerospace, and industrial components, such as brake systems, pistons, bearings, turbine blades, and sliding elements.

References

[1] Samal P, Vundavilli PR, Meher A, Mahapatra MM. Recent progress in aluminum metal matrix composites: A review on processing, mechanical and wear properties. J Manuf Process. 2020;59:131-52. https://doi.org/10.1016/j.jmapro.2020.09.010

[2] Ajay CV, Moshi AAM. Investigation and Optimization of the Tribological Parameters of Hypoeutectic A356/Gr/Sn Metal Matrix Composites Using Grey-Fuzzy and ANN Modeling Methods. J Fail Anal Prev. 2024;24(4):1916-33. https://doi.org/10.1007/s11668-024-01978-8

[3] Jegan G, Kavipriya P, Sathish T, Singaravelu D, Lawrence TS, Vino T. Synthesis, mechanical, and tribological performance analysis of stir-casted AA7079: ZrO2 + Si3N4 hybrid composites by Taguchi route. Adv Mater Sci Eng. 2021;2021:1-12. https://doi.org/10.1155/2021/7722370

[4] Soundararajan R, Sathishkumar A, Sivasankaran S, Shanthosh G, Karthik S. Evaluation of Microstructures, Mechanical and Dry-Sliding Wear Performance of A356-(Fly Ash/SiCp) Hybrid Composites. Int J Met Cast. 2022;16(4):2079-96. https://doi.org/10.1007/s40962-021-00731-3

[5] Kaviyarasan K, Soundararajan R, Raj A, Kannan SA, Ayyankalai P. Assessment of Mechanical and Tribological Characteristics of A356 Reinforced with x wt% CaB6 Composites. J Inst Eng India Ser D. 2022;103(1):75-84. https://doi.org/10.1007/s40033-021-00303-z

[6] Pandey V, Chakraborty K. The Applications of ANOVA and Taguchi-Fis Simulation for Performance Evaluation of Machining Parameters and Subsequent Parametric Optimization During Dry Turning of A356 (Al-Si) Alloy. In: Lecture Notes in Mechanical Engineering. 2023; 1-11. https://doi.org/10.1007/978-981-19-2188-9_1

[7] Deepak Kumar S, Dewangan S, Ghose J, Jha SK. Optimization of EDM process parameters of thixoformed A356-5TiB2 in situ composites. Mater Sci Forum. 2020;271-6. https://doi.org/10.4028/www.scientific.net/MSF.978.271
[8] Annapoorna K, Shobha R, Bharath V, Rajanna S, Manjunath V, Madeva N, Auradi V, Shivaprasad CG . Optimization of stir casting parameters for the tensile behavior of nano Al2O3 and ZrO2 reinforced Al-Mg-Si alloy metal composites. Res Eng Struct Mater. 2025;11(2):631-46. http://dx.doi.org/10.17515/resm2024.292ma0518rs
[9] Abolusoro OP, Khoathane MC, Mhike W. Influence of melon shell ash reinforcement on the mechanical and microstructural characteristics of recycled aluminium matrix composites. Res Eng Struct Mater. 2025;11(2):783-98. http://dx.doi.org/10.17515/resm2024.320me0614rs
[10] Milojević S, Stojanović B. Determination of tribological properties of aluminum cylinder by application of Taguchi method and ANN-based model. J Braz Soc Mech Sci Eng. 2018;40(12):571. https://doi.org/10.1007/s40430-018-1495-8
[11] Shabana S, Shafeeq MA, Jajimoggala S, Lakshmi VVK, Kolluri S. Evaluation of Mechanical, Tribological, and Corrosion Properties of AA6083 with Zirconia Addition. J Bio Tribocorros. 2025;11(2):53. https://doi.org/10.1007/s40735-025-00976-z
[12] Ali Z, Nagaral M, Muthuraman V, Auradi V, Bharath V, Kumar S, et al. Synthesis of a356 alloy-variable particle sized boron carbide composites: investigations on mechanical behaviour and tensile fractography. aeletters. 2024;9(3):162-72. https://doi.org/10.46793/aeletters.2024.9.3.4
[13] Jayakumar K. Comparative Study of Ball Nose and Flat End Milling on A356 Alloy/SiCp Metal Matrix Composite. In: Lecture Notes in Mechanical Engineering. 2021; 487-95. https://doi.org/10.1007/978-981-15-4745-4_43
[14] Arunbharathi R, Arish R, Girith Chandru S, Bhavandharshan K, Gowthamprasath AD, Hari K. Application of Desirability Approach to Determine Optimal Turning Parameters. SAE Tech Pap. 2024. https://doi.org/10.4271/2024-01-5022
[15] Pugalenthi T, Arulraj M, Sowrirajan M, Vijayan S. Impact of stir-squeeze casting process parameters on tensile strength of hybrid aluminium matrix composite. Proc Inst Mech Eng Part E J Process Mech Eng. 2022;236(6):2589-98. https://doi.org/10.1177/09544089221095663
[16] Shirani A, et al. PEO-Chameleon as a potential protective coating on cast aluminum alloys for high-temperature applications. Surf Coat Technol. 2020;397. https://doi.org/10.1016/j.surfcoat.2020.126016
[17] Ashok Kumar MS, Ajit Prasad SL. Wear Characteristics of Hybrid Aluminium MMCs Subjected to Extrusion Process. IOP Conf Ser Mater Sci Eng. 2021.
[18] Ramasubbu N, Kulandaivel D, Raj JA. Influence of Different Squeeze Pressures on Metallurgical and Tribological Behavior of A356 Silicon Carbide and MoS2-Based Hybrid Composites. J Inst Eng India Ser D. 2024. https://doi.org/10.1007/s40033-024-00763-z
[19] Ajay Kumar K, Mallikarjuna C. Wear behavior of A356/ Al2O3/MoS2 hybrid nanocomposites. Mater Today Proc. 2022;54:409-14. https://doi.org/10.1016/j.matpr.2021.09.470
[20] Jibin Bose TC, Sudev Babu C, Rajeev VR, Hashim M. Effect of temperature on the tribological characteristics of A356/15 wt.% SiCp functionally graded composites in unidirectional contact. Mater Today Proc. 2023. https://doi.org/10.1016/j.matpr.2023.02.200
[21] Li H, Lu S, Xu P, Jiao L, Yang J, Wu D. Microstructure and tribological properties of in-situ formed Al3Zr/A356 composite. Mater Res Express. 2020;7(5). https://doi.org/10.1088/2053-1591/ab8d65
[22] Raghul KS, Kaviyarasan K, Vinayagamoorthi MA, Velmurugan S. Evaluation of Tribological Behaviour of Stir Casted Aluminium Alloy Hybrid Composites. SAE Tech Pap. 2024. https://doi.org/10.4271/2023-01-5171
[23] Li H, et al. Surface Wear Behavior and Friction and Wear Mechanism Studies of A356/3 wt.% Al3Zr Composites. J Mater Eng Perform. 2021;30(5):3892-902. https://doi.org/10.1007/s11665-021-05707-2
[24] Soundararajan R, Sivasankaran S, Babu N, Adhithya GPR. Appraisal of tribological properties of A356 with 20% SiC composites under dry sliding condition. J Braz Soc Mech Sci Eng. 2020;42(3). https://doi.org/10.1007/s40430-020-2231-8
[25] Jiao L, et al. Microstructure and tribological behavior of in situ ZrB2/A356 composites prepared under magnetic field. Surf Topogr. 2021;9(1). https://doi.org/10.1088/2051-672X/abe720
[26] Liu T, Hu M, Ran Q, Jiang B, Ji Z, Zhou X. A Novel Al-Ti-C-B-Ce Alloy Preparation Process and Its Refinement Effect to A356 Alloy. JOM. 2024;76(1):379-86. https://doi.org/10.1007/s11837-023-06258-8
[27] Deepak Kumar S, Dewangan S, Ghose J, Jha SK. Optimization of EDM process parameters of thixoformed A356-5TiB2 in situ composites. Mater Sci Forum. 2020;271-6. https://doi.org/10.4028/www.scientific.net/MSF.978.271
[28] Pujar CV, Manihalla PP. An experimental investigation of mechanical properties of Al-7.25Si-0.45Mg alloy. AIP Conf Proc. 2020. https://doi.org/10.1063/5.0007104

[29] Szablewski P, Smak K, Krawczyk B. Analysis of the Impact of Wiper Geometry Insert on Surface Roughness and Chips in Machining Materials Used in the Aviation Industry. Adv Sci Technol Res J. 2022;16(1):203-12. https://doi.org/10.12913/22998624/143475
[30] Seeman M, Sivaraj P, Seetharaman R, Ashok Kumar I. Analysis and Optimization Of Machining Parameter During Turning Of A356/10%Sicp MMC Using Response Surface Methodology Approach. IOP Conf Ser Mater Sci Eng. 2020. https://doi.org/10.1088/1757-899X/961/1/012014
[31] Chen H, Gao Q, Wang Z, Fan Y, Li W, Wang H. Optimization of Casting System Structure Based on Genetic Algorithm for A356 Casting Quality Prediction. Int J Met Cast. 2023;17(3):1948-69. https://doi.org/10.1007/s40962-022-00902-w
[32] Çalışkan O, Sunar T, Özyürek D. Mechanical and wear performance of A356/Al2O3 aluminum nanocomposites by considering the mechanical milling time and microstructural properties. Ind Lubr Tribol. 2023;75(4):465-73. https://doi.org/10.1108/ILT-02-2023-0031
[33] Yadav AK, Gautam G, Mohan S. Prediction of tribology in (Mg2Si+TiB2)/A356 composites based on RSM method and correlative with topographical characteristics. Phys Scr. 2023;98(11). https://doi.org/10.1088/1402-4896/acf9e9
[34] Prathap Singh S, Ananthapadmanaban D. Effect of Silicon Nitride Particles on the Sliding Wear Characteristics of Functionally Graded Aluminium Composite. J Mater Eng Perform. 2024;33(6):2875-96. https://doi.org/10.1007/s11665-023-09011-z
[35] Pani D, Surekha B, Ranjan R, Samal P, Rao SR, Mishra PC. Effect of Electrode Material Variations on Wear Characteristics of Stir Cast A356/Red Mud/TiC Hybrid Metal Matrix Composite During Electrical Discharge Machining. Tribol Ind. 2024;46(4):560-9. https://doi.org/10.24874/ti.1642.03.24.05
[36] Davim JP. Statistical and computational techniques in manufacturing. Springer Sci Bus Media; 2012. https://doi.org/10.1007/978-3-642-25859-6
[37] Ajay Kumar K, Mallikarjuna C. Microstructure and mechanical properties of A356/Al2O3/MoS2 hybrid nanocomposites. Mater Today Proc. 2022;54:415-20. https://doi.org/10.1016/j.matpr.2021.09.472
[38] Singh A, Kumar K, Sundari KG, Ranjan R, Surekha B. Experimental investigations and multi criteria optimization during machining of A356/WC MMCs using EDM. Decis Sci Lett. 2022;11(2):147-58. https://doi.org/10.5267/j.dsl.2021.12.001
[39] Arunadevi M, et al. Optimization Process to Develop Tungsten Carbide Reinforced with Aluminium MMCs Using Surface Plots and ANN. J Inst Eng India Ser D. 2024. https://doi.org/10.1007/s40033-024-00693-w
[40] Prathap Singh S, Prabhuram T, Elilraja D, Durairaj JI. Influence of Drilling Operation Variables on Surface Roughness and Thrust Force of Aluminium Reinforced with 10% Al2O3 Functionally Graded Metal Matrix Composite. In: Lecture Notes in Mechanical Engineering. 2022. p. 65-73. https://doi.org/10.1007/978-981-16-4222-7_8
[41] Sunil Kumar M, Sathisha N, Jagannatha N, Chandra BT. Tribological Study on Effect of Chill Casting on Aluminium A356 Reinforced with Hematite Paticulated Composites. J Bio Tribocorros. 2022;8(2). https://doi.org/10.1007/s40735-022-00635-7
[42] Gajević S, Marković A, Milojević S, Ašonja A, Ivanović L, Stojanović B. Multi-Objective Optimization of Tribological Characteristics for Aluminum Composite Using Taguchi Grey and TOPSIS Approaches. Lubricants. 2024;12(5). https://doi.org/10.3390/lubricants12050171
[43] Dewangan S, Sharma SK, Vishvakarma AK, Tiger C. Analysis of Productivity and Surface Characteristics of A356-TiB2 Nanocomposites in EDM. In: Lecture Notes in Mechanical Engineering. 2023. p. 749-58. https://doi.org/10.1007/978-981-19-4606-6_69